A Concertina−Shaped Vibration Energy Harvester−Assisted NFC Sensor With Improved Wireless Communication Range

Kankana Paul, Dinesh R. Gawade, *Student Member, IEEE*, Roy B. V. B. Simorangkir, *Member, IEEE*, Brendan O'Flynn, *Senior Member, IEEE,*, John L. Buckley, *Member, IEEE,*, Andreas Amann, Saibal Roy

***Abstract*—The explosive growth of wireless sensor platforms and their emerging wide range of application areas make the development of a sustainable and robust power source, an essential requirement to enable widespread deployment of these wireless devices. As a solution to this cardinal issue, this paper reports the design and fabrication of a resonant Vibration Energy Harvester (VEH) that comprises interleaved springs, manifesting a concertina shaped structure that can enable large mechanical amplitudes of oscillation. Within a relatively small footprint ($9cm^3$), this concertina-VEH yields a large power density of $455.6\mu W/cm^3g^2$ while operating at a resonant frequency of 75Hz. Additionally, the feasibility of the implemented VEH to support NFC based wireless sensor platform, that is yet uncharted, is also investigated in this work. A very low-power consumption Near Field Communication (NFC) wireless sensor node has been designed and developed for this purpose. The developed concertina VEH has been employed to power the electronics interface of this NFC sensor. Using mechanical energy derived from as low as 0.2g excitation, our study shows that the VEH can enhance the electromagnetic interaction between the transmitting antenna and the reader, resulting in a 120% increase in wireless communication range for the NFC sensor node. Such a high-performance energy harvester assisted NFC sensor node has the potential to be used in a wide range of Internet of Things (IoT) platforms as a reliable and sustainable power solution.**

***Index Terms*—Concertina Spring, Electromagnetic Transduction, Internet of Things, NFC sensor, Vibration Energy Harvester, Wireless Communication.**

I. Introduction

THE drive towards building pervasive intelligence encompassing urban as well as rural environments has paved the way for the Internet of things (IoT) [1], which has reshaped our regular lifestyle alleviating the dependence on wired communication systems since its inception [2]. The inexorable advancement in low to ultra-low power electronics have steered the rapid growth of the IoT platform expanding into several application fields including disaster management [3], agriculture [4], industrial monitoring [5], wearable motion sensing [6] and condition monitoring [7], to name a few. With the ongoing implementation of 5G (Fifth generation) and the emergence of 6G (Sixth generation) wireless technology on the horizon, the explosive growth of IoT connected devices reinforces the requirement of a robust and reliable power solution for the deployed wireless communication platforms. Utilizing distributed clean energy sources, especially the ubiquitous mechanical energy available in environment through dedicated transducers in the form of vibration energy harvesters to power the IoT-based wireless sensor platforms is a sought-after alternative of batteries in forthcoming IoT applications [8], [9], [10], [11], [12].

Over the past couple of decades, the surge of research in the field of mechanical energy harvesting from ambient vibrations through electromagnetic transducer underpins the simplicity of implementation of this harvester with a spring-mass-damper system [13] along with high mechanical energy extraction efficiency at resonance [14]. For the classical linear type Vibration Energy Harvesters (VEHs), the response from the harvester maximizes at resonance when the frequency of excitation equals the natural frequency of oscillation of the energy harvesting unit. The external excitation provided to this harvester translates into relative displacement between the magnet and coil and induces an extractable voltage across the coil terminals. Hence, enhancing the range of mechanical displacement is a potential route to enhance the efficiency of the linear VEH devices at or close to the resonant frequency. Nonlinear spring compliance incorporated into the spring geometry has been exploited in the field of VEHs to widen the operable bandwidth of frequencies [10], enabling the harvester suitable for harnessing mechanical energy from broadband vibrations. Mallick et al., reported an FR4 based nonlinear VEH that exploits the nonlinear spring stretching effect (cubic-hardening stiffness) and demonstrates a 5 times improvement in the operable bandwidth of frequency [15]. However, the cubic-hardening stiffness based nonlinear effects strengthen only at higher amplitudes of excitation, which puts a critical limit on the viability of these nonlinear VEHs for relatively weaker vibrations that are predominantly present in bridges, air conditioning systems, trams, and trains, etc. [16], [17], [18], [19]. Additionally, depending on the nature of vibration, higher power generation through the nonlinear VEHs are not always guaranteed [20]. However, by virtue of offering wider bandwidth of operable frequencies, instead of peak power delivered for specific frequencies like the linear VEHs, the nonlinear VEHs are promising in providing substantially large average power density over a broadband of frequencies [21] (random vibrations) as compared with the linear VEHs.

Kankana Paul, Dinesh R. Gawade, Roy B. V. B. Simorangkir, Brendan O'Flynn, John L. Buckley, Saibal Roy are with Micro-Nano-Systems Center at Tyndall National Institute, Lee Maltings, Dyke Parade, Cork, Ireland

Andreas Amann is with the School of Mathematical Science, University College Cork, Cork, Ireland

Saibal Roy is additionally with the Department of Physics, University College Cork, Cork, Ireland

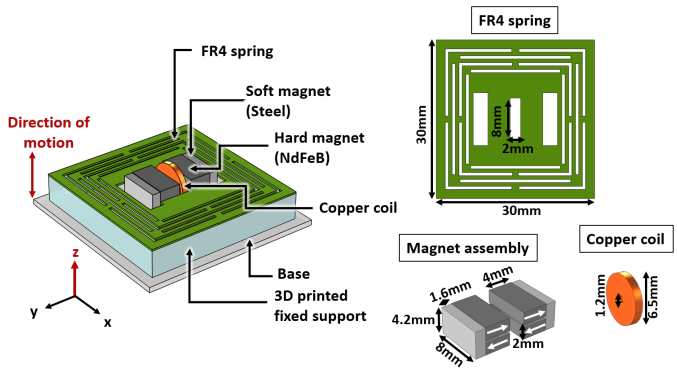

Fig. 1. Schematic of the conceived Electromagnetic vibration energy harvester. The red arrow indicates the out-of-plane motion of the VEH.

On the other hand, the linear type VEHs employing high-efficiency transducers have been used both in academia [22], [23], [24], [25], [26] and in the industry [8], [27] as a robust and reliable solution to the powering issue of wireless sensor platforms. This class of VEH offers large deliverable power at resonance, at the cost of considerably low bandwidth of operable frequencies. However, with an intelligent design strategy, frequency tuning [28] and prior knowledge of the vibration characteristics of the site of deployment [29], the VEH could be designed to trigger the resonance, which effectively results in larger power generation. Qiu et al., presented an electromagnetically transduced resonant VEH exploiting Halbach assembly of magnets which enhances the electromagnetic interaction and maximizes the output power to 90.35mW with 0.5g excitation and at a low frequency of resonance (12.65Hz) [30]. Although this device has great potential for powering a wireless sensor platform, however, this comes at the cost of a large footprint (volume of the device, calculated $164.27cm^3$). Gao et al., experimentally investigated the performance of resonant VEHs in transducing mechanical energy from wheel-set/track of railways [31]. The device delivers 119 mW power at 6Hz resonance for a 1.2-2mm rail track displacement, but occupies a large footprint of $1680cm^3$, which puts a critical limit on its wide range of applicability. Recently Rubes et al., presented an autonomous wireless sensing and communication platform powered through an electromagnetic vibration energy harvester that resonates at 33Hz with harmonic excitation [32]. The energy harvesting system drives a wireless sensor node to deliver 600 samples of data per second at the cost of a considerably large volume of $124cm^3$. Owing to the geometry of the linear springs, these resonant harvesters perform characteristically small displacements around the point of static equilibrium, which restricts large amplitudes of oscillation for small excitation amplitude. Hence, a key challenge is to develop linear resonators within a small footprint that exhibits large amplitudes of oscillations even for smaller excitations, while demonstrating linear spring-force variation.

From the application perspective, amongst the popular wireless communication platforms such as NB-IoT (Narrow-Band Internet of Things), SigFox (a French global network provider), LoRaWAN (Long Range Wide Area Network), BLE (Bluetooth Low Energy) and NFC (Near Field Communication), the NFC technology offers a unique benefit of a very low power requirement [33] while transmitting data. Recent studies have reported that typically, $900\mu W$ of power is consumed by NFC-based sensor interfaces while offering a communication range up to 4.5cm [34], [35], [36], [37]. The communication range of NFC platform largely depends on the several parameters such as reader type, NFC antenna size, coupling between NFC reader and tag, RFID air interface and power consumption of the front-end electronics. With NFC type 5 enabled smartphone as a reader, a maximum communication range of 7cm could be achieved, which increases to 1 m when a 13.56MHz reader (ISO/IEC 15693) is employed [34], [38]. Nowadays, the inclusion of NFC technology in smartphones enables on-call data acquisition through reader/smartphones, which substantially reduces the installation cost of the NFC sensors [34], [39]. This allows frictionless migration of the data from the edge to the cloud, which paves the way for a number of low communication-range applications such as health monitoring [40], food quality monitoring [41], gas monitoring [42], structural health monitoring [43] etc. Battery assisted NFC sensor node offers enhanced communication range [35]. As the battery powers the front-end electronics associated with the sensor node, the power harvested through the NFC aids in communicating the data-modulated signal by strengthening the electromagnetic interaction between NFC antenna and the reader. However, the degradation of battery life owing to thermal/mechanical stress as well as chemical reactions [44] poses a great challenge in the usage of batteries for NFC sensor nodes. Hence, assisting the NFC with an energy harvester to power the sensor hardware and to enhance the range of communication appears to be a viable approach that would open wider fields of application.

In this work, we present a novel resonant VEH demonstrator and provide a feasibility study on its potential for supporting wireless sensor platforms to achieve the above-discussed goal. We designed and developed a linear interleaved spring on FR4 material that comprises two linear springs arranged in series, offering a relatively low natural frequency of oscillation ($<$200 Hz) with a small footprint, while exhibiting large out-of-plane oscillations at resonance. Section II outlines the design guidelines and fabrication of the resonant VEH structure that extracts mechanical energy through electromagnetic transduction. Resembling the shape of the musical instrument 'concertina', the fabricated spring exhibits large displacements while demonstrating linear spring-force characteristics [45], [46]. The electrodynamical characterization of this concertina-VEH is presented in Section III. The resistive load optimization and the frequency response of the VEH for a fixed optimized load have been discussed. Large deformation of the 'concertina' spring translates into enhanced voltage induction through the magnet-coil assembly that results in large power delivered across a suitable load for low excitation. As a concept demonstrator, we have designed and developed a low-power NFC sensor node that has been described with functional block diagrams in Section IV. In Section V we demonstrate the efficacy of the developed VEH to power the front-end electronics of the NFC sensor, which strengthens the

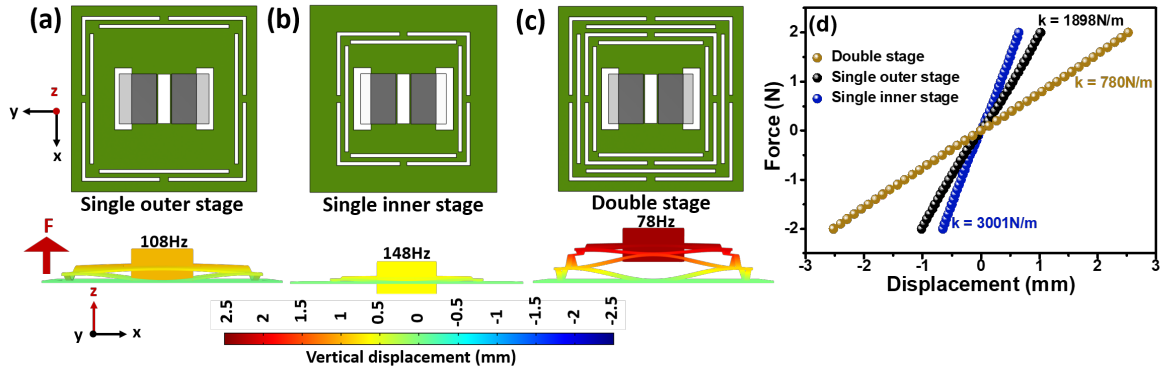

Fig. 2. The design of concertina springs with (a) single stage on the outer side, (b) single stage on the inner side, and (c) double stage springs in series. All have been shown along with the displacement profile for an applied force F. (d) The comparison of the spring force-displacement characteristics for the designed springs.

electromagnetic interaction between the transmitter antenna and the receiver, resulting in an enhanced range of communication. Finally in section VI, through an exhaustive comparison we demonstrate the efficacy of the developed VEH in extracting energy from weak vibrations and powering wireless sensor platform offering improved range of communication. Such a system could be exploited in a wide range of IoT based applications, e.g. temperature and humidity monitoring of industrial cleanroom environment while extracting mechanical energy from installed Air Conditioning systems.

TABLE I
COMPARISON OF SPRING MATERIALS AND ASSOCIATED PROPERTIES OF EMVEH SPRINGS

Spring material	Young's modulus	Spring type	Resonant frequency	Max. Disp.
Silicon [47]	*170-190GPa	MEMS	143 Hz 156Hz	0.409 mm 0.351 mm
Silicon-on -insulator [48]	180GPa	MEMS	367 Hz 587Hz	$\sim$ 125 μm (0.5 N) $\sim$ 80 μm (0.5 N)
Nickel[49]	165GPa	MEMS	648 Hz	100 μm (50 mN)
Copper foil [50]	128GPa	Micro-scale	371 Hz	142.4 μm (resonance)
Electroplated copper [51]	*110-130GPa	MEMS	94.5 Hz	259.1 μm (resonance)
PDMS [52]	360kPa	MEMS	93 Hz	$\sim$ 110μm (1.3μN)
FR4 this work	21GPa	Macro scale	75 Hz	2500 μm 2N

*Typical values of Young's modulus of Silicon and Electroplated Copper taken

II. DESIGN AND FABRICATION OF THE CONCERTINA VEH

Typically, an electromagnetic VEH structure comprises a mechanical resonator or a spring that vibrates in response to an externally applied mechanical excitation, and a magnet-coil assembly that is employed to facilitate the electromagnetic transduction. Figure 1 shows the proposed VEH comprising a spring structure that holds an assembly of magnet on the central stage. The spring is fixed to a rigid support on the base through the outer perimeter and the rest of the spring is suspended and allowed to vibrate. Close to the magnet, a rigidly fixed coil is inserted vertically. On external excitation, the spring vibrates in the vertical direction which enables the magnets to exhibit out-of-plane displacements with respect to the fixed coil, inducing voltage across the coil. In this work, the concertina spring architecture is laser micromachined on a 300μm thick FR4 sheet. FR4 stands for the low-cost 'Flame retardant' materials that are popularly used in printed circuit boards (PCBs) and a wide range of electrical and electronics applications owing to the electrical insulation properties. The low Young's modulus (approximately 21-24GPa) of the FR4 material aids in scaling the natural frequency of oscillation of the resonator down, enabling the VEH to efficiently harness mechanical energy from ambient vibration sources as a significant fraction of this energy is distributed over the low-frequency domain (<200Hz)[16], [19]. In addition to the above, the FR4 sheet derives mechanical strength from the constituent interwoven fibreglass, which results in mechanically robust VEH structures. In the literature, FR4 based spring structures have been tested in laboratory vibration environment for more than 10 million cycles [53] without any mechanical failure. In another reliability test [54], FR4 device has been subjected to 100MPa stress and has been mechanically stable for up to 250 million cycles of operation. Table I shows the comparison of different spring constituent materials. The modulus of elasticity (Young's modulus) parameter, which directly influences the dominant frequency of oscillation of the spring structure, is compared for different materials including Silicon, Silicon-on-Insulator, Nickel, Copper, Alloy, PDMS and FR4. The Young's modulus of PDMS (360kPa) and FR4 (21GPa) structures are significantly lower than the rest of the materials, which, in turn, aids in bringing the frequency of

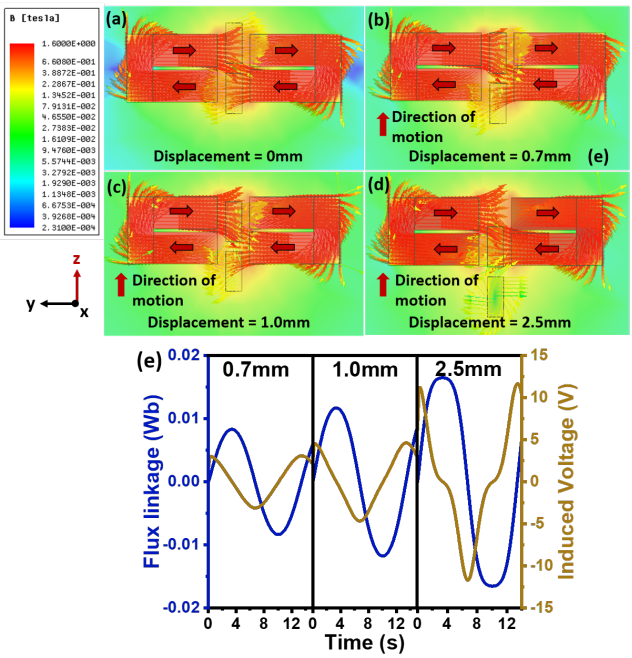

Fig. 3. The electromagnetic interaction between the coil and the magnet assembly and the corresponding variation of magnetic field lines have been shown in (a) for no displacement, (b) for 0.7 mm displacement, (c) for 1 mm displacement and (d) for 2.5 mm displacement of the magnets from the equilibrium position. (e) The variation of magnetic flux linkage and the induced voltage for different displacement of the magnet.

oscillation down to a lower frequency range. However, designing intricate springs on PDMS that would exhibit large out-of-place displacements, could be challenging considering the mechanical stability and durability of the spring architecture. Hence, considering the mechanical robustness, low cost, and low elasticity modulus we have chosen FR4 as the spring constituent material for the resonant VEH.

Four sintered Neodymium-Iron-Boron (NdFeB) magnets are epoxy bonded on the central stage (16mm × 10mm) of the FR4 spring such that oppositely polarized magnets are on each side of the 8mm × 2mm slot at the centre dedicated for the coil, as shown in Fig.1. To intensify the magnetic flux gradient around the coil, soft magnetic steel keepers are used to guide the magnetic flux from the oppositely polarized pair of magnets which aids in forming a closed path of magnetic field lines through the coil. A miniaturized copper wire-wound coil (outer and inner diameter 6.5mm and 1.2mm respectively, thickness 1mm, 2500 turns and 700Ω resistance) is inserted through the dedicated slot. To keep the coil stationary with respect to the magnets, it is fixed with the base platform through a 3D printed fixture.

The spring architecture is designed with the motivation of increasing the out-of-plane compliance to enhance the electromagnetic interaction and hence the extractable electrical energy. The outer dimension of the spring is 30mm × 30mm. The width of each spring arm is 0.7mm. As shown in Fig.2(a), a single stage of the spring (outer), which comprises four sets of springs, instigates vertical out-of-plane displacement of the central load owing to the interleaved spring architecture. Resembling the shape of the musical instrument 'concertina', we call these concertina springs. With a single-stage concertina spring (on the outer side), the VEH exhibits small out-of-plane displacements, as shown in Fig.2(a), when excited at 108Hz which is the natural frequency of oscillation of the structure. Approximately 2N external force is required to displace the load 1mm normal to the plane. These characteristics manifest a rather stiff spring, yielding a spring stiffness coefficient of 1898N/m. On the other hand, a single-stage concertina spring on the inner side makes the spring even stiffer and allows the central load to displace only 0.7mm for a similar level of force at 148Hz frequency of oscillation, resulting in a large spring stiffness coefficient of 3001N/m (Fig.2(b)). The small-displacement exhibited by the single-stage spring restricts the coil from experiencing large magnetic flux variation resulting from the displacement of the magnet assembly.

Adding the interleaved concertina springs in series could potentially enhance the out-of-plane compliance by offering a reduced equivalent spring stiffness (k_{eq}) as compared with the individual single stage of springs [55]. As shown in Fig.2(c), the second set of concertina springs that are connected in series with the first stage of springs are relatively smaller. The spring stiffness coefficient of the double stage concertina topology reduces to 780N/m, which is much lower than the stiffness that each of the individual concertina stages offers. The interleaved structure of the spring instigates larger out-of-plane displacements for similar external excitation compared with the rest of the spring topologies, as shown in Fig.2(d). Arranging these concertina springs in series also helps to scale the frequency of oscillation down from 148Hz to 78Hz. In this context, it is to be noted that the patterns and especially the length of the spring (the width of each spring is fixed to 0.7mm) plays a key role in influencing the spring stiffness and the frequency of oscillation of the structure. This can be verified by revisiting Fig. 2(b), that has the shortest length of springs resulting in larger spring stiffness and higher frequency of oscillation. In contrast with this, the spring with a single stage on the outer end (Fig. 2(a)) demonstrates larger compliance and lower frequency owing to the longer springs, which is further enhanced when two stages of springs are used together in the double stage concertina design (Fig. 2(c)) that efficiently reduces the spring stiffness as well as the frequency of oscillation. Adding more of such interleaved spring stages could potentially scale down and tune the natural frequency of oscillation of the spring structure as well as further enhance the amplitude of displacement. However, that comes at the cost of increased footprint of the VEH device. Moreover, very large displacement of the spring from the position of static equilibrium could cast adverse effect on the electromagnetic interaction and hence on the deliverable power, since at very large displacements the magnetic field lines emerging from these small magnets would be too feeble for the coil to interact with. Hence, we limit our study up to the double stage of concertina-springs.

Ansys Maxwell has been employed as the finite element analysis tool to investigate the electromagnetic interaction between the coil and the magnet assembly for the different spring topologies using single stage and double stage concertina springs, considering open circuit conditions. Following

Faraday's law, the relative motion between the coil and the magnet induces a voltage V into the coil which depends on the magnetic flux ϕ and can be represented as,

$$V = -N\frac{d\phi}{dt} = -N\frac{d\phi}{dz}\frac{dz}{dt} \tag{1}$$

Where, N is the number of turns of the coil. Therefore, a larger gradient of magnetic flux would result in higher induced voltage and power. Figure 3(a) shows the magnetic flux distribution when the VEH is stationary. The arrows indicate the direction of magnetization as well as the magnetic flux lines. The soft magnet blocks on both sides of the magnets aid in routing the magnetic flux lines in a way that intensifies the flux distribution across the coil that is placed at the centre. The maximum obtainable out-of-plane displacement has been considered to study the magnetic flux linkage with the coil and the induced voltage into the coil. With a single stage of concertina spring at the inner side (as shown in Fig.2(b)) of the spring topology, the maximum displacement is 0.7mm, which allows 8mWb magnetic flux linkage, resulting in a maximum of 4V induced voltage across the coil. This improves when the concertina spring is placed at the outer side of the spring design (maximum displacement 1mm), the magnetic flux linkage enhances to 11mWb and proportionately the induced voltage increases to 6V, as shown in Fig.3(e). The magnetic flux linkage maximizes to 16.5mWb with double stage concertina springs design that offers large out-of-plane displacement (2.5mm). Fig.3(d) shows that with 2.5mm displacement, the coil segments experience a drastic change of magnetic flux lines through them, yielding a large magnetic flux gradient. This reflects onto the improved induced voltage of 11.2V. Hence, we have selected the double stage concertina springs for further analysis and experiments.

The solid mechanics module of COMSOL multiphysics has been used to investigate the modes of vibration of the designed double concertina VEH. We consider here only the first three eigenmodes at 78Hz, 156Hz and 247Hz (Fig.4). The first mode corresponds to the out-of-plane displacement of springs, and the other two modes manifest tilts occurring at higher frequencies. The large difference in frequency of the consecutive modes of vibrations indicates that the concertina springs architecture restricts the torsion or tilts in the system dynamics and promotes the desired out-of-plane vibrations which would aid to enhance the efficiency of the VEH in harnessing mechanical energy.

III. Experimental Characterization of the VEH and Discussions

The electromechanical characteristics of the conceived VEH have been investigated with Bruel and Kjær Shaker unit that comprises of LDS V455 permanent magnet shaker, LDS vibration controller, PA1000L power amplifier and a DeltaTron 4517-002 piezoelectric accelerometer mounted on the shaker to monitor the amplitude of excitation and feedback the signal to the controller. The controller in turn generates a signal that is fed to the power amplifier, which then amplifies the signal and sends the drive current signal to the shaker for generating the desired vibrations. The VEH is mounted on the shaker and

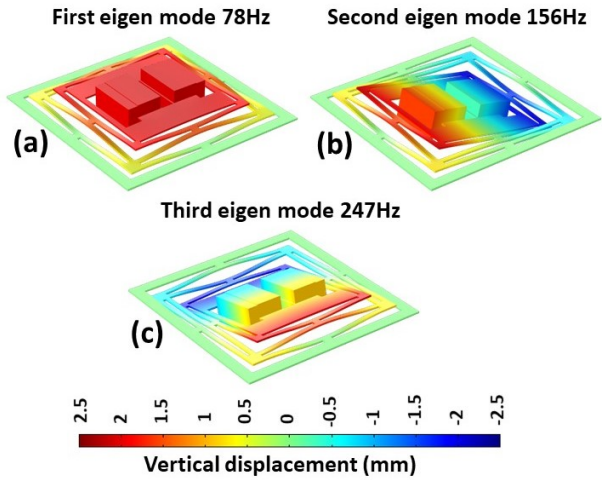

Fig. 4. The first three modes of oscillation of the concertina spring structure: (a) at 78 Hz, (b) at 156 Hz, and (c) 247 Hz. The out-of-plane and torsional modes of vibrations have been portrayed.

excited with harmonic vibrations of fixed amplitudes (e.g. 0.1g to 1g) while the frequency of the excitation is swept from 65Hz to 85Hz with a constant sweep rate of 1Hz/sec. The induced voltage across the coil of the VEH is recorded with a digital oscilloscope (Picoscope 3000series). The experimental setup is shown in Fig.5.

The frequency of resonance of the VEH is found to be 75Hz from the initial frequency sweeps in the open circuit conditions, which is slightly lower than 78Hz resonance as we obtained through the finite element analysis. To quantify the sharpness of resonance, or in other words, the linearity of the system, the Q-factor of this VEH has been measured using the ring-down method [56]. The VEH has been excited at the resonant frequency with 0.5g amplitude of harmonic vibrations. The decay of the response is observed once the excitation is withdrawn. The open-circuit Q-factor is represented as,

$$Q_{OC} = \frac{\pi f_0 \Delta t}{\ln \frac{V_1}{V_2}} = \frac{1}{2\rho_m} \tag{2}$$

where, f_0 is the frequency of resonance, V_1 and V_2 are the voltages at the limits of the time interval Δt, and ρ_m is the mechanical damping ratio that is inversely proportional to the Q_{OC}. Using this relation, the Q_{OC} is measured to be 546.17, which in turn indicates a low mechanical damping ratio of 0.0009. These two factors are majorly dependent on the design of the spring and could be further tailored by altering the design.

A suitable resistive load is often connected across the VEH to extract the usable electrical energy for the target applications. In this case, the VEH is driven at the resonant frequency with a fixed amplitude of excitation 0.5g, and the resistive load across the VEH is varied from 200Ω to 10kΩ to find the optimal load condition that will result in maximum power extraction from the VEH. As shown in Fig.6(a), the power delivered across the resistance maximizes for 1kΩ load and the delivered power peaks at 1.02mW for 0.5g excitation. On increasing the value of the load resistance further, the

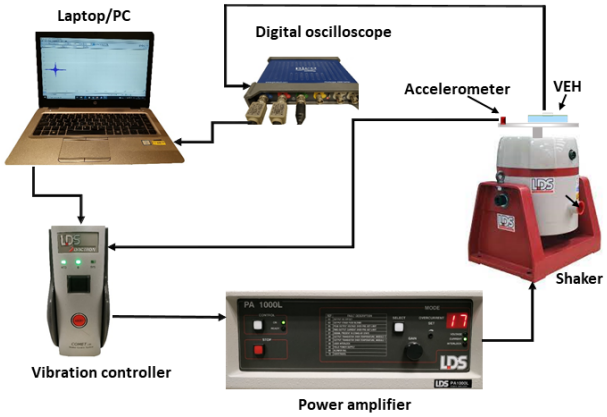

Fig. 5. Schematic of the experimental setup for the electrodynamic characterization of the developed linear concertina-VEH.

power gradually drops and the voltage saturates at 1.9V for a load of 10kΩ. The variation of the power delivered across the optimal load 1kΩ with respect to the frequency of excitation, for different amplitudes of the drive has been investigated. For very low amplitudes of excitation, such as 0.1g, the VEH delivers a low peak load power of 46μW at 75Hz (Fig.6(b)). On increasing acceleration, the VEH generates more electrical power while resonating at 75Hz. The VEH delivers a maximum of 2.9mW power when the amplitude of excitation increases to 1g, offering a half-power bandwidth of 1.16Hz. The inset of Fig.6(b) shows the variation of the obtainable power at 75Hz as a function of the amplitude of excitation. It is noticeable that the power increases steeply with the acceleration, with approximately a rate of 300μW of additional power for increasing the acceleration by 0.1g. The high out-of-plane compliance of the double stage concertina spring structure aids in enhancing the electromagnetic interaction, which translates into large extractable power from a considerably small footprint.

IV. Design and Fabrication of the NFC based Sensor Node

The objectives of target application primarily influence the selection of wireless technology. NB-IoT, SigFox, LoRaWAN, WiFi, and ZigBee are among popular commercial wireless communication solutions that offer long range of communication at the cost of higher transmission power requirement. However, the widespread usage of smartphones that typically comprise embedded BLE and NFC plays a key role behind the popularity of these two wireless technologies, which allows on-call data acquisition wirelessly within a shorter communication range. In particular, NFC technology, that has been used for this work, is a short-range and contactless communication technology that outperforms BLE in terms of power requirement. We summarize and compare the key performance metrics of the different wireless technologies in Table II.

NFC technology exploits inductive coupling between two loop antennas in close proximity to facilitate reliable data

TABLE II
Comparison of Wireless Communication Technologies

Wireless Technology	Wireless comm. range(m)	DC Sleep current (μW)	Tx RF power (mW)	Reference (mW)
NB-IoT	10000	10	252-900	[58], [59]
SigFox	10000	2.1	66	[58], [60]
LoRaWAN	5000	2.2	103-264	[58], [61]
WiFi	250	13.2	775.7	[58], [62]
ZigBee	100	2.97	115-152	[58], [63]
BLE	20	2.91	21.12	[64], [65]
NFC	0.07	2.34	0.198	[38]

communication, and operates within the worldwide available unlicensed radio frequency band of 13.56MHz [57]. A block diagram of a battery-less NFC temperature and relative humidity sensor with a reader (in this case NFC type 5 enabled smartphone) is shown in Fig.7. The role of the smartphone in this setup is to wirelessly power the sensor and also to wirelessly read the data that the sensor generates. In principle, upon placing the smartphone near the NFC sensor hardware, the time-varying electromagnetic fields generated from the NFC transmitter of the smartphone (shown in Fig. 7(a) through the signal symbol) induces current into the NFC loop antenna in the sensor hardware through inductive coupling. A fraction of the harvested RF power is employed to power the front-end electronics of the sensor and the remaining power is used to facilitate the communication of the data acquired by the sensor through the NFC radio. The detailed process is illustrated in Fig.7(a). As shown, the loop antenna feeds the induced RF power to the NFC radio transceiver. The RF front-end of this NFC radio consists of energy harvesting circuitry, which converts the harvested RF power into the DC voltage. Following this RF-DC conversion, a low dropout voltage regulator (LDO) is used to regulate this incoming DC voltage into a steady DC supply (i.e., 1.8VDC) for the following sensor electronics stage e.g. the microcontroller unit (MCU), the sensor, and all other circuitry. Once the required power is received, the sensor is activated and can function to measure the target physical parameters such as temperature, relative humidity, and so on. Through I2C protocol the sensor communicates this acquired data with the microcontroller unit using the remaining RF power that was harvested through the smartphone. This data is then written into the user area of NFC radio's dual access non-volatile memory (EEPROM) and it is read through the smartphone wirelessly using the dedicated read command. The time taken by the NFC sensor node from harvesting the power from the reader to communicating the data back to the reader is often referred as tapping time, which is dependent on the microcontroller computational speed and the data transmission rate. The voltage and clock settings have been optimized (i.e., Clock source = Multispeed internal oscillator clock, MCU peripheral clock (f_{CLK}) = 0.524MHz, I2C core input clock (f_{I2CIN}) = 1.028MHz, core voltage (V_{CORE}) = 1.2V, and supply voltage (V_{DD}) = 1.8V) considering the trade-off between the computational speed and DC power consumption. The DC power required by the NFC sensor hardware to be fully functional is measured to be 597μW which is considerably reduced with respect to the

previously reported value of 900μW [34]. Our developed NFC sensor (Fig.7(b)) requires a minimum tapping time of 6.79 s.

The NFC sensor hardware prototype is shown in Fig.7(b), which comprises a loop antenna and following commercial off-the-shelf (COTS) components: an NFC radio (ST25DV16K-JFR6D3), MCU (STM32L031K6U6), LDO (STLQ015M18R) from STMicroelectronics, as well as temperature and humidity sensors (SHTC3) from Sensirion AG. The sensor hardware uses a standard 0.8mm thick 4-layer FR4 substrate. The detailed operation of the developed NFC sensor hardware with a smartphone, along with its performance characteristics, including the power consumption (0.9mW), wireless communication range (4.5cm), and sensor characterization, has been reported by the authors in [34].

In this work, we exploit the mechanical energy harvesting capability of the developed concertina VEH to power the front-end electronics of the NFC sensor hardware. The functional block diagram of the NFC sensor hardware assisted with the developed VEH is given in Fig.8(a). The NFC sensor along with the AC-DC rectification unit is shown in Fig.8(b). By connecting the VEH energy harvester, the RF energy harvested from the smartphone can be focused to facilitate the communication of the data acquired by the sensor back to the smartphone. The VEH would act as a sustainable power source, that offers the capability of continuously providing power to the electronics interface to support the NFC sensor hardware, as a replacement of batteries that only offer limited lifetime. To pair the NFC sensor with the developed VEH, further optimizations have been performed on the hardware and the firmware of the previously reported NFC sensor. To allow for an extraction of sufficient electrical energy even from a low amplitude vibration, a double-stage voltage multiplier circuit [66], [67] comprising of two capacitors (10μF each) and two diodes (Small-signal Schottky Diode, part number BAT85-T/R) has been employed for the rectification of the incoming AC signal from the VEH. Following the rectification stage, a 560μF (20V) conductive polymer aluminium solid capacitor (SEPF series) has been added to store the energy and to supply it to the NFC sensor hardware circuitry when required. The voltage regulator is activated upon receiving a minimum voltage of 2.66V from the VEH. This regulator then provides a steady 1.8V DC supply to the rest of the associated sensor electronics. To maintain the overall footprint of the system small, the voltage multiplier circuit along with the storage capacitor has been implemented on a PCB board mounted on top of the remaining electronics of the NFC sensor node with a vertical spacer. Upon the VEH integration (Fig. 8), the tapping time of the NFC sensor node has decreased from 6.79 s to 1.95s. This shorter tapping time might be attributed to the VEH supplying an adequate power to the electronics to perform continuous data acquisition and processing. Hence, the 'tapping time' only accounts for the time taken for communicating the processed data to the reader.

V. Feasibility Experiment of Battery-less and VEH Assisted NFC Sensor Node Platform

In this section, we demonstrate the significance of the developed concertina VEH that is implemented to assist the developed NFC sensor node platform representing an autonomous wireless platform system. The experimental set-up used in this study is depicted in Fig.9(a). The VEH is mounted on the shaker unit which emulates ambient mechanical vibrations in a laboratory environment. The shaker unit is covered with a plastic casing and on top of it a communication range measurements set-up for the developed NFC hardware has been placed, which comprises a base that holds the NFC sensor hardware, and a movable stage that carries the reader (smartphone). 'NFC for iPhone' and 'Simply NFC' application interfaces have been used to read the data from the NFC sensor. This set-up is used to vary the distance between the NFC loop antennas in the sensor hardware and that of the smartphone. The AC-DC rectifier stage, as mentioned in the previous section, has been fabricated on copper strip-board and mounted on top of the NFC hardware to minimize the length of the wired connections and to reduce the footprint. The output of the VEH is connected to the input of the rectifier stage through wired connections.

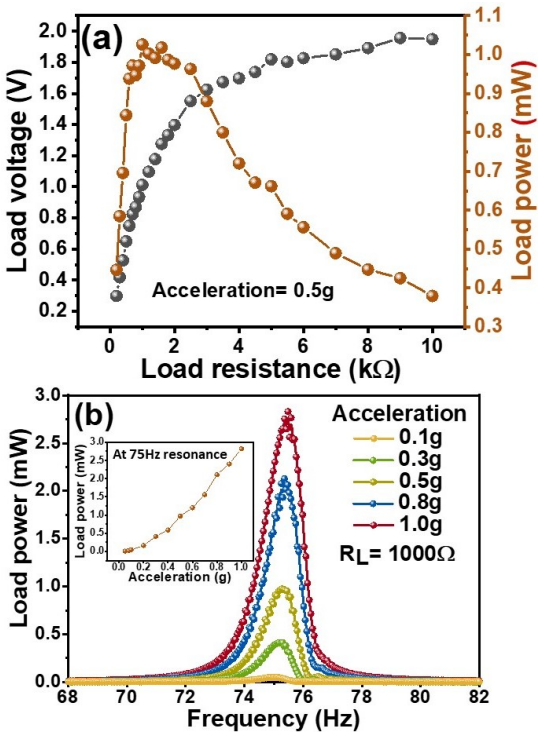

Fig. 6. (a) The variation of load voltage and power delivered across the load with respect to the variation of the resistive load for the developed linear VEH with concertina springs that is shown at the inset. (b) The variation of the power delivered across the optimized resistive load as the frequency of excitation is varied. The Inset shows the level of powered delivered to the load as a function of the amplitude of acceleration.

Upon applying a harmonic excitation on the VEH at the resonant frequency (75Hz), the extracted electrical energy passes through the rectification stage and is stored into the load capacitor. Fig.9(b) shows the variation of the rectified signal when the NFC sensor interface is connected to it as a load. We have selected this capacitor for its fast charging capability. The amplitudes of the excitation is varied from 0.2g to 0.6g that typically represents the amplitudes of vibrations that can be

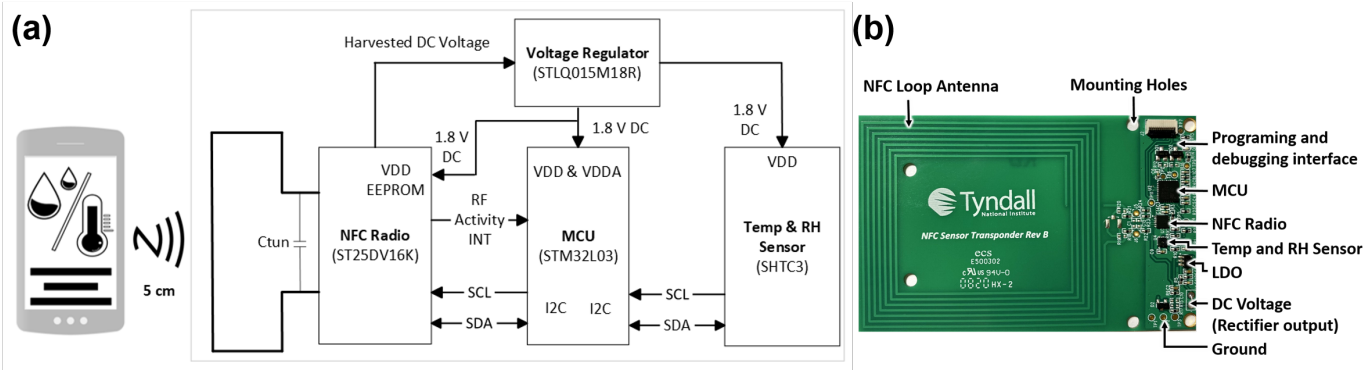

Fig. 7. (a) The functional block diagram of the NFC sensor hardware. (b) The developed NFC sensor hardware [34]

experienced on, for instance, clothes drying machine, blending machine, and car dashboard [68],[69] etc. As shown in the inset of Fig.9(b), the capacitor takes approximately 30s to charge from 0 to 2.66V, when such a low vibration amplitude of 0.2g is employed. Once the voltage input to the NFC sensor hardware exceeds 2.66V, the integrated low dropout voltage regulator (LDO) enters into the active state and provides a steady DC supply of 1.8V to the following circuitry comprising of the microcontroller, temperature-humidity sensor along with the NFC radio transceiver. If the NFC reader (in this case a smartphone) is in the vicinity of the NFC sensor hardware, the data packet from the sensor is transmitted through the NFC radio to the reader. The energy drawn to facilitate this communication brings the voltage across the capacitor down from 2.66V to 2.4V which puts the microcontroller and the sensors back into off mode until the capacitor charges back to 2.66V. In the case of 0.2g vibration, this occurs over a 4.7s time interval. This charging and discharging of the capacitor reflects onto the rectified voltage as ripples, as shown in Fig.9(b).

As described in Section IV, for the conventional passive NFC tags, the energy received from the reader/smartphone by the tag loop antenna, which is translated into a regulated 1.8V DC, is partly employed to power the electronics in the NFC sensor hardware and partly for communicating (EPROM) the data-modulated signal back to the reader. The fraction of the power left for the latter then determines the strength of the load-modulated signal or equivalently the communication range of the NFC tags. For the NFC sensor hardware used in this work, it provides a communication range of 5cm when not connected to any additional source of energy. In the case of VEH-assisted NFC tag, the VEH supplies the power required by the electronics. Therefore, the NFC sensor hardware can retain the RF power harvested from the reader fully for communicating back the sensing data-modulated signal to the reader and hence provides a larger communication range, i.e., 11cm or 120% improvement as shown in Fig.10(a).

Figure10(b) shows the variation of the deliverable power of the VEH as a function of the amplitude of excitation. The power required by the NFC sensor hardware to be fully functional is measured to be 597μW (shown by the blue dots). It is noticed that with 0.2g drive amplitude, 164μW power can be extracted across the load resistance of 1kΩ. Such a low vibration is investigated to be sufficient to support the NFC sensor leading to an increased communication range, though with longer capacitor charging time from 2.4V to the required 2.66V (see Fig.9(b)). The obtainable energy from the VEH increases with increasing amplitude of the external excitation. Since a larger power of 598μW is delivered when the VEH is excited with 0.4g acceleration (matching the required power level of the NFC sensor hardware), the capacitor charges faster between 2.4V to 2.66V , shortening the charging time to 1.2s as shown in Fig.9(b), while extending the communication range up to 11cm. It is interesting to note that by further increasing the amplitude of excitation, e.g. for 0.6g, the VEH provides substantial energy which drives the NFC sensor hardware interface autonomously, thereby implementing a sustainable power source to support the NFC hardware. In Fig.9(b) the steady supply from the rectification stage (green line) indicates that the capacitor at this stage would no longer be required to store and supply energy to the circuitry associated with the NFC.

VI. Comparison with the State-of-the-art VEHs and Envisaged IoT Application

A comparison of the performance of the developed VEH with the state-of-the-art VEHs has been presented in Table III. The key parameters of comparison are the footprint of the VEH device used to power the wireless platform, the amplitude of excitation, the power density (delivered power per unit volume per unit excitation) and the charge storage capacitor. The table shows that, in terms of the footprint, the developed VEH device outpaces all the rest of the devices. Additionally, the device starts to power the wireless sensor node at a very low level of acceleration which makes this suitable for a wide range of IoT based application scenarios. The wireless communication system has also been developed and optimized carefully to minimize the power consumption so that the autonomous wireless platform with enhanced communication range is functional even for weak vibrations. To the author's best knowledge, this work is a first of its nature presenting a detailed feasibility study of combining high efficiency vibration energy harvester with emerging NFC technology to implement a robust and sustainable wireless communication platform for IoT applications.

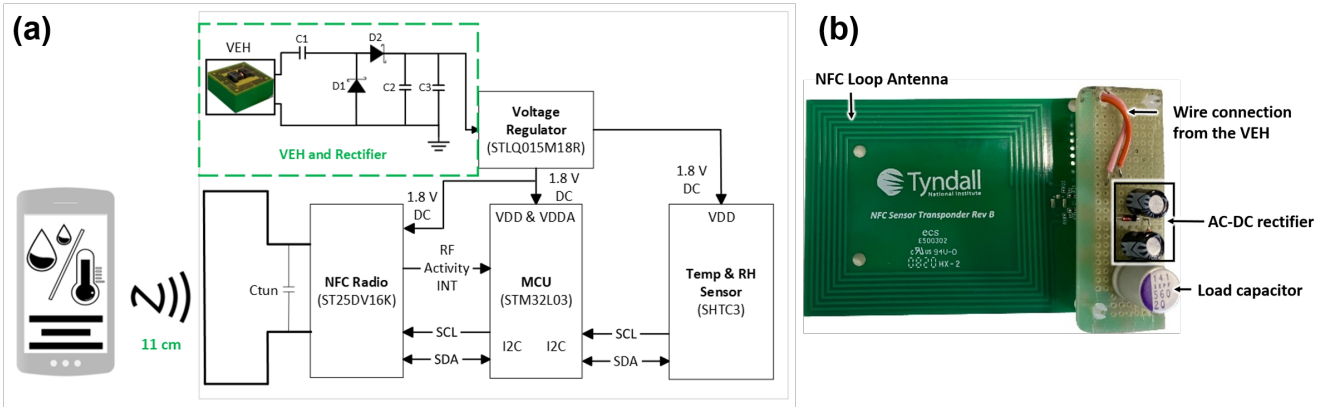

Fig. 8. (a) The functional block diagram of the NFC sensor hardware when assisted with the developed concertina VEH. (b) The developed NFC sensor hardware along with the AC-DC rectification stage integrated to facilitate the rectification of incoming AC voltage from the VEH.

TABLE III
PERFORMANCE COMPARISON OF THE DEVELOPED PROTOTYPE WITH THE REPORTED VEHS

Ref.	Excitation (g)	Resonant frequency(Hz)	Volume (cm^3)	Delivered power (μW)	Power density ($\mu W/cm^3g^2$)	Communication protocol	Load capacitance(μF)
EM (resonant) [32]	$\sim$ 0.5	33	123.75	$\sim$ 800	25.8	Radio Transceiver Short-burst 2.4GHz proprietary	23.5
EM (resonant) [31]	3	6	420	119000	31.5	No demonstration with wireless sensor platform	680
PE (resonant) [29]	0.25	100	200	$\sim$ 4000	320	Radio Transceiver	500
PE (resonant) [26]	0.2	39,110	NA	$\sim$ 3800	NA	Radio Transceiver	100
EM (resonant) [24]	$\sim$ 0.5	28,40	$\sim$ 206	6500	126.2	No demonstration with wireless sensor platform	NA
EM+TE (resonant) [12]	0.6	4.5	$\sim$ 29.3	10070	954.7	Directly powered portable electronics	22
EM (resonant) [11]	0.73	13	$\sim$ 93	980	19.77	LoRaWAN and BLE	Supercapacitor
This work	0.2	75	9	164	455.6	NFC	560
This work	0.6	75	9	1200	370.36	NFC	Not required

Note: EM- Electromagnetic, PE- Piezoelectric, TE-Triboelectric, NA- Not Available

As demonstrated, the developed concertina-VEH is sensitive to low levels of vibrations which enables this energy harvesting system to transduce mechanical energy even from the weak vibrations, opening up the scope for exploiting this benefit in some niche application areas. For example, in the context of industrial cleanroom environments, continuous monitoring of temperature and relative humidity, and maintaining their variation range between 18-21°C and 30-50% respectively is an imperative requirement for minimizing microbial growth, static charge build up, delicate equipment damage as well as for the users comfort [70]. The Heating, Ventilation, and Air Conditioning (HVAC) units installed inside the cleanroom offers substantial mechanical energy distributed around the resonant frequency of the concertina-VEH [19], [71]. In the context of the above mentioned application scenario, the mechanical energy from HVAC system will be consistently available since the HVAC in a clean-room has to be operational all the time to keep the contaminants at a minimum, which ensures perpetual mechanical energy extraction through the concertina-VEH. This opens up the scope for installing the developed concertina-VEH on the HVAC systems which would enable the harvester to generate substantial energy. The delivered power through the harvester could be employed to power the electronics interface of the NFC based sensor node, while enhancing the range of communication of the NFC node. Hence, the developed NFC sensor node could report on the vital physical parameters of the cleanroom environment while being assisted through the concertina-VEH which would harness mechanical energy from the ceiling HVAC units.

The presented concertina spring topology offers the unique scope of tuning the natural frequency of oscillation of the device by adding more stages of concertina springs. Such flexibility could be well exploited for niche application area such as harnessing mechanical energy from human body by

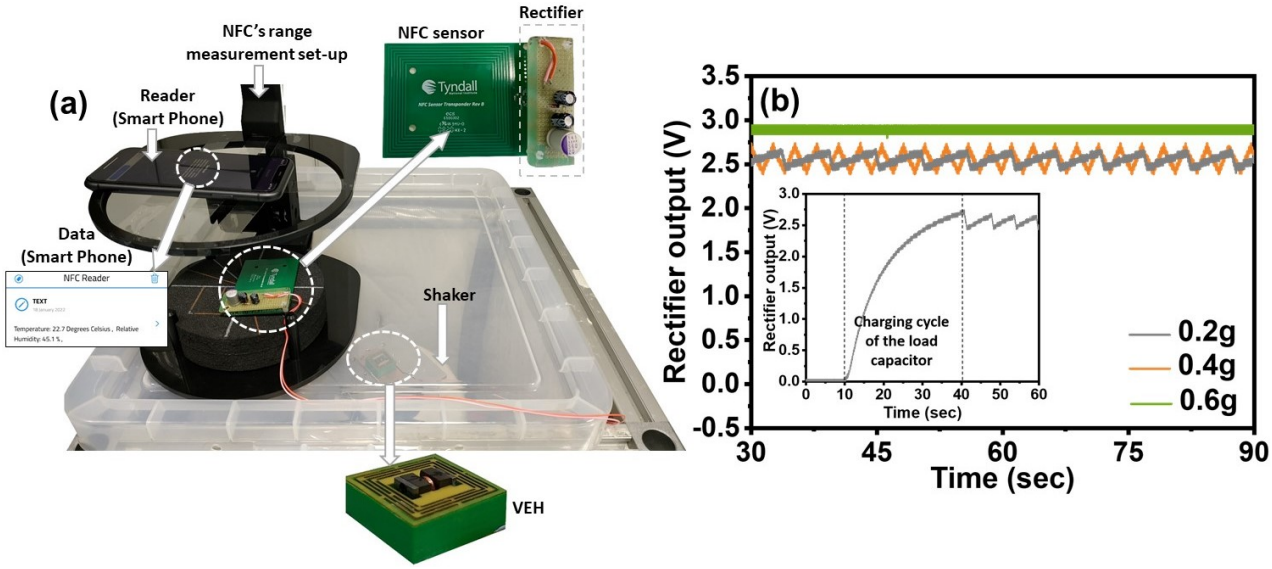

Fig. 9. (a) The experimental set-up of employing the developed VEH to support the NFC sensor hardware. The VEH is placed on the shaker under the cover. (b) The variation of the rectified voltage across the load capacitor for different amplitudes of excitation of the VEH. The inset shows the fast charging cycle of the load capacitor used in this experiment.

scaling down the frequency, typically less than 10Hz, through additional stages of concertina springs. NFC sensor system could be implemented on flexible material [72], [73] for the ease of integration on human body. The concertina VEHs together with flexible NFC sensor system could implement a sustainable and robust wireless platform for human health monitoring. The successful demonstration of the developed concertina VEH supporting the constructed NFC sensor node also implies a possible avenue to implement the VEH for other types of wireless communication platform. This includes those based on the far-field communication (e.g., [74] and [75]) to allow for the development of a sustainable and robust wireless sensing systems with an even higher communication range.

VII. Conclusion

A battery-less Vibration Energy Harvester (VEH) assisted NFC (Near Field Communication) sensor node has been reported. The resonant FR4 based VEH comprises interleaved springs that are connected in series, building a concertina shape that exhibits a large amplitude of displacement (2.5mm) within a small footprint of $9cm^3$ when subjected to external excitation. Owing to this enhanced out-of-plane compliance, the VEH offers a large power density of $455.6\mu W/cm^3g^2$ when operating at the resonance. This makes the concertina-VEH a potential candidate for assisting the developed low power consuming NFC sensor node. With the VEH powering the electronic interface of the sensor node, the electromagnetic interaction between the transmitting antenna and the reader embedded in smartphone enhances which in turn brings a 120% improvement in the range of communication of this wireless sensor node. The excellent dynamic response of the concertina-VEH enables it to effectively harness mechanical energy even from weaker vibrations (e.g. 0.2g harmonic excitation). For lower amplitudes of excitation, a storage capacitor of 560μF has been used to provide a steady DC

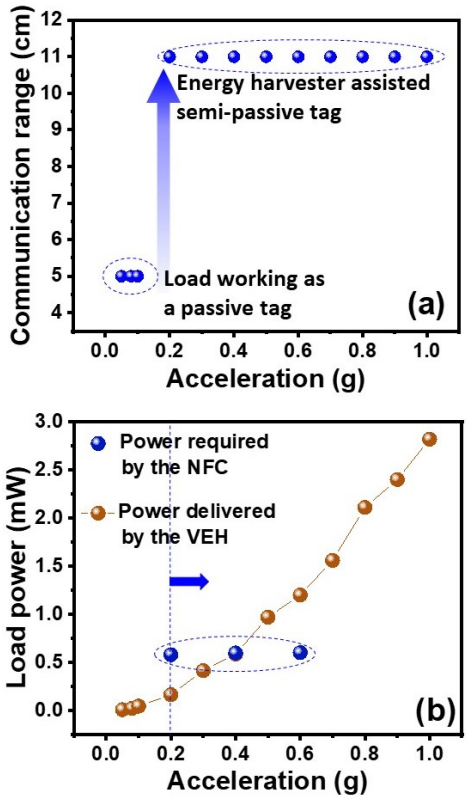

Fig. 10. The variation of the power delivered by the VEH across the optimized load has been shown in (a)Demonstrates the communication range the NFC hardware provides as a function of the amplitude of excitation of the VEH. (b)The blue points show the power consumption of the NFC sensor hardware when the amplitude of excitation for the VEH changes from 0.2g to 0.6g.

supply to the sensor interface. But for moderate acceleration levels (0.6g), the concertina-VEH generates considerably large power (1.2mW), making the capacitor redundant for steadily powering the sensor electronics.

ACKNOWLEDGMENTS

This work is financially supported by a platform research grant from "CONNECT"- a strategic research centre on 'Communication and Future Network-sustainable IoT' funded by the Science Foundation Ireland (SFI) and is co-funded under the European Regional Development Fund Grant Number 13/RC/ 2077_P2. This is also part funded by a EU Horizon 2020 research and innovation programme project 'Enables', Project ID: 730957. We would also like to acknowledge funding support from the European Union's Horizon 2020 research and innovation program for APACHE project under grant agreement number 814496.

REFERENCES

[1] A. Zanella, N. Bui, A. Castellani, L. Vangelista and M. Zorzi, "Internet of Things for Smart Cities", *IEEE Internet of Things Journal*, vol. 1, no. 1, pp. 22-32, 2014.

[2] K. Ashton, "That 'internet of things' thing," *RFID journal*, vol. 22, no. 7, pp. 97-114, 2009.

[3] A. Adeel, M. Gogate, S. Farooq, C. Ieracitano, K. Dashtipour, H. Larijani, A. Hussain, "A Survey on the Role of Wireless Sensor Networks and IoT in Disaster Management", in *Geological Disaster Monitoring Based on Sensor Networks*, Springer, 2018.

[4] F. Akhter, H. R. Siddiquei, M. E. E. Alahi, and S. C. Mukhopadhyay, "Design and development of an IoT-enabled portable phosphate detection system in water for smart agriculture", *Sensors and Actuators A: Physical*, vol. 330, p. 112861, 2021.

[5] L. Zhao, I. B. M. Matsuo, Y. Zhou, and W. Lee, "Design of an Industrial IoT-Based Monitoring System for Power Substations", *IEEE Transactions on Industry Applications*, vol. 55, no. 6, pp. 5666-5674, 2019.

[6] H. Huang, X. Li, S. Liu, S. Hu and Y. Sun, "TriboMotion: A Self-Powered Triboelectric Motion Sensor in Wearable Internet of Things for Human Activity Recognition and Energy Harvesting", *IEEE Internet of Things Journal*, vol. 5, no. 6, pp. 4441-4453, 2018.

[7] P. Li, Z. Long and Z. Yang, "RF Energy Harvesting for Batteryless and Maintenance-Free Condition Monitoring of Railway Tracks", *IEEE Internet of Things Journal*, vol. 8, no. 5, pp. 3512-3523, 2021.

[8] Perpetuum Rail Applications (July 7, 2022). [Online]. Available: https://perpetuum.com/applications/rail/

[9] M. Koca, G. Gurbilek, B. Soner and S. Coleri, "Empirical Feasibility Analysis for Energy Harvesting Intravehicular Wireless Sensor Networks", *IEEE Internet of Things Journal*, vol. 8, no. 1, pp. 179-186, 2021.

[10] K. Paul, A. Amann, and S. Roy, "Tapered nonlinear vibration energy harvester for powering Internet of Things", *Applied Energy* , vol. 283, p. 116267, 2021.

[11] J. C. Rodriguez, V. Nico, and J. Punch, "A Vibration Energy Harvester and Power Management Solution for Battery-Free Operation of Wireless Sensor Nodes", *Sensors* , vol. 19, no. 17, 2019.

[12] M. Salauddin, R. M. Toyabur, P. Maharjan, and J. Y. Park, "High performance human-induced vibration driven hybrid energy harvester for powering portable electronics", *Nano Energy*, vol. 45, pp. 236-246, 2018.

[13] D. Mallick, P. Constantinou, P. Podder, and S. Roy, "Multi-frequency MEMS electromagnetic energy harvesting", *Sensors and Actuators A: Physical*, vol. 264, pp. 247-259, 2017.

[14] L. Zuo, B. Scully, J. Shestani, and Y. Zhou, "Design and characterization of an electromagnetic energy harvester for vehicle suspensions", *Smart Materials and Structures*, vol. 19, no. 4, p. 045003, 2010.

[15] D. Mallick, A. Amann, and S. Roy, "A nonlinear stretching based electromagnetic energy harvester on FR4 for wideband operation", *Smart Materials and Structures*, vol. 24, no. 1, p. 015013, 2014.

[16] Y. Zhao, X. Ling, Z. Wang, W. Gong, and G. Li, "Acceleration Frequency Characteristics of the Freight-Train-Induced Vibration of the Beijing-Harbin Railway Subgrade", *Shock and Vibration*, vol. 2020, 2020.

[17] C. Pronello, "Analysis of tram-induced vibrations affecting roads and buildings in standard urban sites", *International Journal of Acoustics and Vibration*,vol. 8, no. 1, pp. 21-29, 2003.

[18] J. T. Gaunt and C. D. Sutton, "Highway bridge vibration studies", *Joint Transportation Research Program*, 1981.

[19] G. Iannace, G. Ciaburro, and A. Trematerra, "Heating, ventilation, and air conditioning (HVAC) noise detection in open-plan offices using recursive partitioning", *Buildings*, vol. 8, no. 12, p. 169, 2018.

[20] P. L. Green, E. Papatheou, and N. D. Sims, "Energy harvesting from human motion and bridge vibrations: An evaluation of current nonlinear energy harvesting solutions", *Journal of Intelligent Material Systems and Structures*, vol. 24, no. 12, pp. 1494-1505, 2013.

[21] D. Zhu and S. Beeby, "A broadband electromagnetic energy harvester with a coupled bistable structure", *Journal of Physics: Conference Series*, vol. 476, no. 1, p. 012070, 2013.

[22] F. M. Foong, C. K. Thein, and D. Yurchenko, "Important considerations in optimising the structural aspect of a SDOF electromagnetic vibration energy harvester", *Journal of Sound and Vibration*, vol. 482, p. 115470, 2020.

[23] L. Dhakar, H. Liu, F. E. H. Tay, and C. Lee, "A new energy harvester design for high power output at low frequencies", *Sensors and Actuators A: Physical*, vol. 199, pp. 344-352, 2013.

[24] M. Perez, S. Chesné, C. Jean-Mistral, K. Billon, R. Augez, and C. Clerc, "A two degree-of-freedom linear vibration energy harvester for tram applications", *Mechanical Systems and Signal Processing*, vol. 140, p. 106657, 2020.

[25] R. Torah, P. Glynne-Jones, M. Tudor, T. O'Donnell, S. Roy, and S. Beeby, "Self-powered autonomous wireless sensor node using vibration energy harvesting", *Measurement Science and Technology*, vol. 19, no. 12, p. 125202, 2008.

[26] S. Lee, B. D. Youn, and B. C. Jung, "Robust segment-type energy harvester and its application to a wireless sensor", *Smart Materials and Structures*, vol. 18, no. 9, p. 095021, 2009.

[27] Data Sheet, Revibe energy harvester (July 7, 2022). [Online]. Available: https://revibeenergy.com/modeld/

[28] D.Mallick, S.Roy, "Bidirectional electrical tuning of FR4 based electromagnetic energy harvesters", *Sensors and Actuators A: Physical*, vol. 226, pp 154-162, 2015.

[29] E. K. Reilly, F. Burghardt, R. Fain, and P. Wright, "Powering a wireless sensor node with a vibration-driven piezoelectric energy harvester", *Smart Materials and Structures*, vol. 20, no. 12, p. 125006, 2011.

[30] J. Qiu, X. Liu, H. Chen, X. Xu, Y. Wen, and P. Li, "A Low-Frequency Resonant Electromagnetic Vibration Energy Harvester Employing the Halbach Arrays for Intelligent Wireless Sensor Networks", *IEEE Transactions on Magnetics*, vol. 51, no. 11, pp. 1-4, 2015.

[31] M. Gao, P. Wang, Y. Cao, R. Chen, and D. Cai, "Design and Verification of a Rail-Borne Energy Harvester for Powering Wireless Sensor Networks in the Railway Industry", *IEEE Transactions on Intelligent Transportation Systems*, vol. 18, no. 6, pp. 1596-1609, 2017.

[32] O. Rubes, J. Chalupa, F. Ksica, and Z. Hadas, "Development and experimental validation of self-powered wireless vibration sensor node using vibration energy harvester", *Mechanical Systems and Signal Processing*, vol. 160, p. 107890, 2021.

[33] D. R. Gawade et al., "A Museum Artefact Monitoring Testbed using LoRaWAN", *IEEE Symposium on Computers and Communications (ISCC)*, pp. 1-3, 2021.

[34] D. R. Gawade et al., "A Smart Archive Box for Museum Artifact Monitoring Using Battery-Less Temperature and Humidity Sensing", *Sensors*, vol. 21, no. 14, 2021.

[35] C. Peres, M. Emam, H. Jafarzadeh, M. Belcastro, and B. O'Flynn, "Development of a low-power underwater nfc-enabled sensor device for seaweed monitoring", *Sensors*, vol. 21, no. 14, p. 4649, 2021.

[36] P. Escobedo, M. Bhattacharjee, F. Nikbakhtnasrabadi, and R. Dahiya, "Smart bandage with wireless strain and temperature sensors and batteryless NFC tag", *IEEE Internet of Things Journal*, vol. 8, no. 6, pp. 5093-5100, 2020.

[37] X. Qian, Z. Li, Z. Meng, N. Gao, and Z. Zhang, "Flexible RFID Tag for Sensing the Total Minerals in Drinking Water via Smartphone Tapping", *IEEE Sensors Journal*, vol. 21, no. 21, pp. 24749-24758, 2021.

[38] Application Note: NFC / RFID, ST25 product overview (July 7, 2022). [Online]. Available: https://www.st.com/content/ccc/resource/sales_and_marketing/presentation/product_presentation/group1/a9/5d/77/96/be/9a/48/7e/ST25_NFC_RFID_product_overview/files/ST25_product_overview.pdf/jcr:content/translations/en.ST25_product_overview.pdf.

[39] D. R. Gawade et al., "A battery-less NFC sensor transponder for museum artefact monitoring-a review of NFC sensor technology and a proposed

solution", *Sensorcomm., International Academy, Research, and Industry Association (IARIA)*, 2019.

[40] P. Escobedo et al., "Smart facemask for wireless CO2 monitoring", *Nature Communications*, vol. 13, no. 1, pp. 1-12, 2022.

[41] R. Raju, G. E. Bridges, and S. Bhadra, "Wireless Passive Sensors for Food Quality Monitoring: Improving the Safety of Food Products", *IEEE Antennas and Propagation Magazine*, vol. 62, no. 5, pp. 76-89, 2020.

[42] P. Escobedo et al., "Flexible Passive near Field Communication Tag for Multigas Sensing", *Analytical Chemistry*, vol. 89, no. 3, pp. 1697-1703, 2017.

[43] C. Strangfeld, S. Johann, and M. Bartholmai, "Smart RFID Sensors Embedded in Building Structures for Early Damage Detection and Long-Term Monitoring", *Sensors*, vol. 19, no. 24, 2019.

[44] X. Hu, L. Xu, X. Lin, and M. Pecht, "Battery lifetime prognostics", *Joule*, vol. 4, no. 2, pp. 310-346, 2020.

[45] D. Grech, K. S. Kiang, J. Zekonyte, M. Stolz, R. J. K. Wood, and H. M. H. Chong, "Highly linear and large spring deflection characteristics of a Quasi-Concertina MEMS device", *Microelectronic Engineering*, vol. 119, pp. 75-78, 2014.

[46] D. Grech, A. Tarazona, M.T. De Leon, K. S. Kiang, J. Zekonyte, R. J. K. Wood, H. M. H. Chong, "A Quasi-Concertina force-displacement MEMS probe for measuring biomechanical properties", *Sensors and Actuators A: Physical*, vol. 275, pp. 67-74, 2018.

[47] Y. Li, J. Li, A. Yang, Y. Zhang, B. Jiang, and D. Qiao, "Electromagnetic vibrational energy harvester with microfabricated springs and flexible coils", *IEEE Transactions on Industrial Electronics*, vol. 68, no. 3, pp. 2684-2693, 2020.

[48] D. Mallick, A. Amann, and S. Roy, "High figure of merit nonlinear microelectromagnetic energy harvesters for wideband applications", *Journal of Microelectromechanical Systems*, vol. 26, no. 1, pp. 273-282, 2016.

[49] S. Sun, X. Dai, Y. Sun, X. Xiang, G. Ding, and X. Zhao, "MEMS-based wide-bandwidth electromagnetic energy harvester with electroplated nickel structure", *Journal of Micromechanics and Microengineering*, vol. 27, no. 11, p. 115007, 2017.

[50] F. Khan, F. Sassani, and B. Stoeber, "Copper foil-type vibration-based electromagnetic energy harvester", *Journal of Micromechanics and Microengineering*, vol. 20, no. 12, p. 125006, 2010.

[51] P. Wang, K. Tanaka, S. Sugiyama, X. Dai, X. Zhao, and J. Liu, "A micro electromagnetic low level vibration energy harvester based on MEMS technology", *Microsystem technologies*, vol. 15, no. 6, pp. 941-951, 2009.

[52] Z. Yang, N. Ismail, C. Son, P. M. Ferreira, and S. Kim, "Broadband, tunable, miniaturized vibration energy harvester using nonlinear elastomer beams and stretchable interconnects", *Advanced Materials Technologies*, vol. 4, no. 12, p. 1900783, 2019.

[53] P. Podder, A. Amann, S.Roy, "A bistable electromagnetic micro-power generator using FR4-based folded arm cantilever", *Sensors and Actuators A: Physical*, vol. 227, pp.39-47, 2015.

[54] G. Hatipoglu, H. Ürey, "FR4-based electromagnetic energy harvester for wireless sensor nodes", *Smart Materials and Structures*, vol. 19, pp.015022, 2009.

[55] G.Aldawood, H.T.Nguyen, H.Bardaweel, "High power density spring-assisted nonlinear electromagnetic vibration energy harvester for low base-accelerations", *Applied Energy*, vol. 253, pp.113546, 2019.

[56] S.P.Beeby, R. Torah, M.J. Tudor, P. Glynne-Jones, T. O'Donnell, C.R.Saha, S. Roy, "A micro electromagnetic generator for vibration energy harvesting", *Journal of Micromechanics and Microengineering*, vol. 17, no. 7, pp. 1257-1265, 2007.

[57] P. White and M. Roland, "Near Field Communication (NFC) Technology and Measurements White Paper", ROHDE & SCHWARZ. [Online]. Available:https://cdn.rohde-schwarz.com.cn/pws/dl_downloads/dl_application/application_notes/1ma182/1MA182_5E_NFC_WHITE_PAPER.pdf.

[58] S. Popli, R. K. Jha, and S. Jain, "A survey on energy efficient narrowband internet of things (NBIoT): architecture, application and challenges", *IEEE Access*, vol. 7, pp. 16739-16776, 2018.

[59] Datasheet: Quectel BC95-G Multi-band NB-IoT Module with Ultra-low Power Consumption (July 7,2022). [Online].Available:https://www.quectel.com/wp-content/uploads/pdfupload/Quectel_BC95-G_NB-IoT_Specification_V1.9.pdf.

[60] Datasheet: "S2-LP Ultra-low power, high performance, sub1 GHz transceiver." (July 7, 2022).[Online]. Available: https://www.st.com/en/wireless-connectivity/s2-lp.html.

[61] Datasheet: CMWX1ZZABZ-078 (July 7, 2022). [Online].Available: https://content.arduino.cc/assets/mkrwan1310-murata_lora_module-type_abz.pdf.

[62] Datasheet: CC3200 SimpleLink Wi-Fi and Internet-of-Things Solution, a Single-Chip Wireless MCU (July 7, 2022). [Online]. Available: https://www.ti.com/lit/ds/symlink/cc3200.pdf.

[63] Application Note: Zolertia RE-Mote (July 7, 2022). [Online]. Available: https://github-wiki-see.page/m/Zolertia/Resources/wiki/RE-Mote

[64] Z. Jianyong, L. Haiyong, C. Zili, and L. Zhaohui, "RSSI based Bluetooth low energy indoor positioning", *International Conference on Indoor Positioning and Indoor Navigation (IPIN), IEEE*, pp. 526-533, 2014.

[65] Nordic Semiconductor, "nRF52840, Product Specification.". (July 7, 2022).[Online]. Available: https://infocenter.nordicsemi.com/pdf/nRF52840 PS v1.2.pdf.

[66] S. Filiz and U. Yunus, "A Comparative Study: Voltage Multipliers for Rf Energy Harvesting System", *Communications Faculty of Sciences University of Ankara Series A2-A3 Physical Sciences and Engineering*, vol. 61, no. 1, pp. 12-23, 2019.

[67] S. S. Chouhan, M. Nurmi, and K. Halonen, "Efficiency enhanced voltage multiplier circuit for RF energy harvesting", *Microelectronics Journal*, vol. 48, pp. 95-102, 2016.

[68] S. Roundy, P. K. Wright, J. Rabaey, "A study of low level vibrations as a power source for wireless sensor nodes", *Computer communications*, vol. 26, pp.1131-1144, 2003.

[69] D. Bhatia, H. J. Hwang, N.D. Huynh, S. Lee, C. Lee, Y. Nam, J.G. Kim, D. Choi, "Continuous scavenging of broadband vibrations via omnipotent tandem triboelectric nanogenerators with cascade impact structure", *Scientific Reports*, vol. 9, pp.1-9, 2019.

[70] T. Sandle, "A Humidex For The Cleanroom: Why Temperature And Humidity Control Matters" (July 7, 2022). [Online]. Available: https://www.ivtnetwork.com/article/humidex-cleanroom-why-temperature-and-humidity-control-matters.

[71] Y. Hu and Y. Xu, "A wideband vibration energy harvester based on a folded asymmetric gapped cantilever", *Applied Physics Letters*, vol. 104, no. 5, p. 053902, 2014.

[72] A. Noda, "Wearable NFC Reader and Sensor Tag for Health Monitoring", *IEEE Biomedical Circuits and Systems Conference (BioCAS)*, pp. 1-4, 2019.

[73] M. Zulqarnain, S. Stanzione, G. Rathinavel, S. Smout, M. Willegems, K. Myny, E. Cantatore, "A flexible ECG patch compatible with NFC RF communication", *npj Flexible Electronics*, vol. 4, no. 1, p. 13, 2020.

[74] S. N. R. Kantareddy, I. Mathews, R. Bhattacharyya, I. M. Peters, T. Buonassisi and S. E. Sarma, "Long Range Battery-Less PV-Powered RFID Tag Sensors", *IEEE Internet of Things Journal*, vol. 6, no. 4, pp. 6989-6996, 2019.

[75] A. Sharif, J. Ouyang, F. Yang, H.T. Chattha, M. A. Imran, A. Alomainy, Q.H. Abbasi, "Low-Cost Inkjet-Printed UHF RFID Tag-Based System for Internet of Things Applications Using Characteristic Modes", *IEEE Internet of Things Journal*, vol. 6, pp. 3962-3975, 2019.

VIII. Biography Section

Kankana Paul received the B.Sc Honours degree in Physics from University of Calcutta in 2012. She secured B.Tech. and M.Tech. degrees in Radiophysics and Electronics engineering from the University of Calcutta, Kolkata, India in 2015 and 2017 respectively. She joined Tyndall National Institute, University College Cork, Ireland in 2017 November as a doctoral research student and she is currently holding that position. Her research interest includes development of Electromagnetic Vibrational Energy Harvester, next-generation magnetic material for CMOS compatible integration with MEMS scale vibration energy harvester, optimization of magnetic performance through analytical and numerical modelling.

Dinesh R. Gawade received a Bachelor's of Technology Degree in 2016 from the Department of Technology, Shivaji University, India in Electronics and Communication Technology. After graduation, he worked in the electronics industry for couple of years as a hardware design engineer from 2016 until 2018. He then worked at the Indian Institute of Technology Mandi, India as a project engineer (Hardware design) before joining Tyndall National Institute, University College Cork, Ireland in 2019. Presently in Tyndall, Dinesh is pursuing a MEngSc degree within the Antenna and RF Design team in the WSN group. His research interest includes development of battery-less sensing devices, low power sensor node, long range wireless sensor network.

Roy B. V. B. Simorangkir (S'15–M'18) received the PhD degree in Electronic Engineering from Macquarie University, Sydney, in 2018. He held a teaching staff position at Macquarie University International College from March 2018 to May 2019. He was also with the Reconfigurable Electronics and Antennas Research Group, Macquarie University as a post-doctoral researcher from September 2018 to December 2018. From May 2019 to May 2020 he worked as a post-doctoral researcher at the Institute of Electronics and Telecommunications of Rennes (IETR), University of Rennes 1. Currently, he is with the Wireless Sensor Networks Group, Tyndall National Institute, University College Cork as a post-doctoral researcher. His general research interests include design and fabrication of flexible antennas and sensors, reconfigurable antennas, and ultra-wideband (UWB) antennas. Dr. Simorangkir is currently serving as a guest editor of a Special Issue of Sensors MDPI Journal and Electronics MDPI Journal. He has been serving as a regular reviewer for several reputable journals in his research field. He was a session chair in the 2018 ACES Symposium, Beijing and the 2021 IEEE International Symposium on Antennas and Propagation (AP-S), Singapore. In 2017, one of his works won first place in the IEEE Region 10 Student Paper Contest, postgraduate category, and was selected as a finalist in the Student Paper and Advanced Practice Paper Competitions of the IEEE MTT-S International Microwave Symposium (IMS), Honolulu.

Brendan O'Flynn (Senior Member, IEEE) received the B.Eng. (Hons.), M.Eng.Sc., and Ph.D. degrees from University College Cork, Ireland, in 1993 and 1995, respectively. He is currently a Senior Staff Researcher with the Tyndall National Institute, Cork, Ireland. He is also the Head of the Wireless Sensor Networks (WSN) Group. His research interests include wearable sensing systems, edge-based analytics, sensor system integration, low power embedded systems design and development, system miniaturization, and RF system design and optimization. He has published widely in these areas and has secured significant funding for the development and deployment of "Smart Sensing" technologies and applied research projects.

John L. Buckley (S'94–M'12) was born in Cork, Ireland. He received the BEng, MEngSc and PhD degrees from the Cork Institute of Technology (CIT) and Department of Electrical Engineering in University College Cork (UCC), Ireland, in 1994, 2004 and 2016 respectively. He was with EMC Corporation, Cork, Ireland, from 1994 to 2002 and joined the Tyndall National Institute, University College Cork in 2005. He is a Senior Researcher and Team Leader for the Antennas and RF Team, WSN Group. His research interests include Antenna design and measurement, Wearable and implantable antenna design and EM and RF circuit modelling for wireless applications.

Andreas Amann received the Diploma degree in physics from the University of Bonn, Germany, and the PhD degree in physics from the Technical University of Berlin, Germany. After being a visiting researcher at the Institute of Applied Optics, Florence, Italy, and a postdoctoral researcher at Tyndall National Institute, Cork, Ireland, he is now a Senior Lecturer in the School of Mathematical Sciences at University College Cork, Ireland. His research interest include nonlinear dynamics, mathematical modelling and machine learning.

Saibal Roy is research professor to the department of Physics, National University of Ireland - University College Cork (UCC) and Head of Micropower Devices and Nanomagnetics research group in Tyndall National Institute. He is Science Foundation Ireland (SFI) Principal Investigator (PI) and a funded investigator in a research center on 'Future communication, network and sustainable IoT - CONNECT'. He is particularly known internationally in the area of integrated high-frequency magnetics for 'power supply on chip', renewable MEMS energy harvesting through electromagnetic transduction (EMT) and demonstration of unconventional magnetic properties in different 'nano-hetero-structures' leading to 'More than Moore' functional devices. Some of his published works on 'Miniaturized vibrational energy harvesting through EMT' have received >2000 citations to date and featured widely in international media. On the other hand, Tyndall 'Magnetics on Si' team successfully licensed the batch-fabricated micro-transformers/micro-inductors capable of operating at 100s of MHz for 'power supply on chip' technology to three major multinational companies with a substantial license fee. In recognition, the team was awarded as the research team of the year by the University. Prof. Roy was awarded the coveted A S Paintal chair professor of engineering, Prof. Tom Brazil excellence in research award, GIAN fellow etc. Prof. Roy has supervised 40 researchers to date, while many of them received different national and international awards and currently holding senior positions in academia as well as in multinational companies. He has 3 granted global patents, authored/co-authored 7 book chapters and published 200 papers in leading journals and conference proceedings, with over 6500 citations and h index of 38 to date.